

# RGM: A Robust Generalist Matching Model\*

Songyan Zhang<sup>1\*</sup>, Xinyu Sun<sup>1\*</sup>, Hao Chen<sup>1</sup>, Bo Li<sup>2</sup>, Chunhua Shen<sup>1</sup><sup>1</sup> Zhejiang University, China    <sup>2</sup> Northwestern Polytechnical University, China

## Abstract

Finding corresponding pixels within a pair of images is a fundamental computer vision task with various applications. Due to the specific requirements of different tasks like optical flow estimation and local feature matching, previous works are primarily categorized into dense matching and sparse feature matching focusing on specialized architectures along with task-specific datasets, which may somewhat hinder the generalization performance of specialized models.

In this paper, we propose a deep model for sparse and dense matching, termed RGM (Robust Generalist Matching). In particular, we elaborately design a cascaded GRU module for refinement by exploring the geometric similarity iteratively at multiple scales following an additional uncertainty estimation module for sparsification. To narrow the gap between synthetic training samples and real-world scenarios, we build a new, large-scale dataset with sparse correspondence ground truth by generating optical flow supervision with greater intervals. As such, we are able to mix up various dense and sparse matching datasets, significantly improving the training diversity. The generalization capacity of our proposed RGM is greatly improved by learning the matching and uncertainty estimation in a two-stage manner on the large, mixed data. Superior performance is achieved for zero-shot matching and downstream geometry estimation across multiple datasets, outperforming the previous methods by a large margin. Code is available at: <https://github.com/aim-uofa/RGM>

## 1 Introduction

Correspondence matching is a fundamental task in computer vision with various applications such as Simultaneous Localization and Mapping (SLAM), multi-view geometry estimation, and image editing. Due to the specific requirements of different applications, recent learning-based matching works are mainly categorized into two branches: *sparse* and *dense* matching. The primary difference is that dense matching, *e.g.*, optical flow estimation, stereo matching, and multi-view stereo matching, is required to provide the matching estimation for each pixel even in occluded regions, while sparse matching is only responsible for finding the corresponding key points, given a pair of images. Besides, in the context of dense matching, the image pairs to be matched typically have limited changes of viewpoint with a relatively small temporal interval while the image pairs for sparse matching normally exhibit more significant changes in viewpoint with various image properties.

Oriented by different applications and requirements, the research of dense and sparse matching has followed separate paths for a long time. Benefiting from the accumulating customized datasets, learning-based approaches have witnessed remarkable improvement for particular tasks such as optical flow estimation (Teed & Deng, 2020; Huang et al., 2022; Sun et al., 2017; Xu et al., 2022b), stereo matching (Zhang et al., 2021; Xu & Zhang, 2020; Chang & Chen, 2018; Xu et al., 2022a), and geometry estimation (Sun et al., 2021; Chen et al., 2022; Ni et al., 2023; Edstedt et al., 2023). However, as discussed in (Truong et al., 2020), the generalization capacity of specialized matching models can often be limited in the case of new scenarios, especially those with large displacements. Some early works (Truong et al., 2020; 2021; Shen et al., 2020; Xu et al., 2023; Li et al., 2020;

\*This work was supported by National Key R&D Program of China (No. 2022ZD0118700). BL's participation was in part supported by National Natural Science Foundation of China (No. 62001394). SZ, XS contributed equally. HC, CS are the corresponding authors.

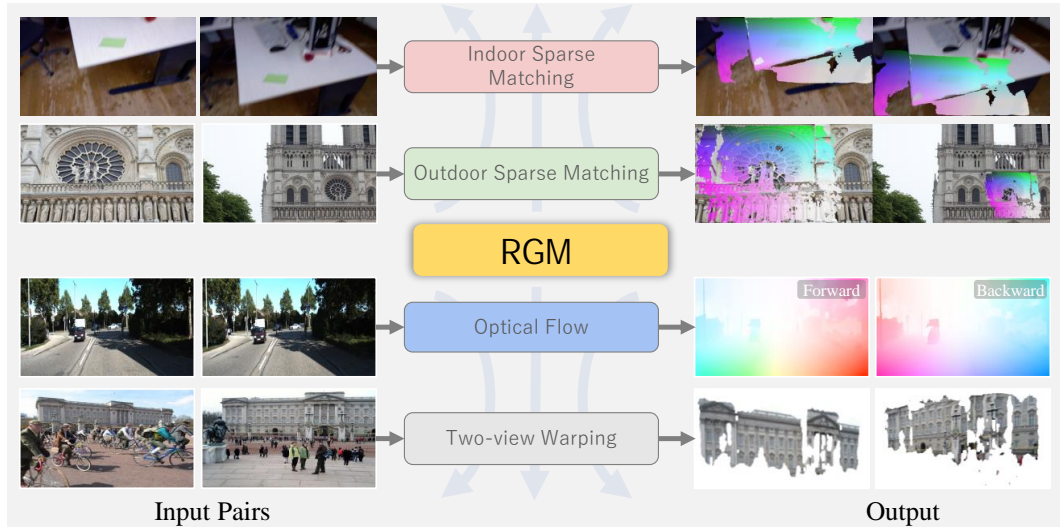


Figure 1: **An illustration of the general capacity of our RGM.** RGM is a robust matching model capable of indoor and outdoor sparse matching even in cases of great displacement or blurred input images. Here, the matched features are indicated by the same color. Moreover, we can also handle the all-paired dense matching such as optical flow estimation and the two-view reconstruction by warping the corresponding pixels to the target view.

[Melekhov et al., 2019](#)) have already made attempts to improve the robustness of matching methods by proposing a universal matching framework capable of both sparse and dense matching.

Despite the improvement in the generalization performance, those universal matching networks still struggle in the performance of specific tasks compared with the specialized models. Besides, how to exploit the advantages of multiple task-specific datasets to boost the robustness of matching is yet to be explored.

It has been revealed that increasing the diversity of training data brings a tremendous improvement in generalization capacity for monocular depth estimation ([Bhat et al., 2023](#); [Yin et al., 2020](#); [2023](#); [Ranftl et al., 2022](#); [Truong et al., 2021](#)). However, the datasets used for dense and sparse correspondence matching show clear domain gaps. Constrained by the difficulty in obtaining fine-grained pixel-wise annotations for dense correspondence matching, most specialized models follow the training pipeline of first pre-training on a large-scale synthesized dataset while fine-tuning on a small-scale real-world dataset. Sparse feature matching tasks for geometry estimation, on the contrary, have an extensive amount of real-world training data ([Li & Snavely, 2018](#); [Dai et al., 2017](#)) but with relatively coarse pixel-wise annotations. Directly training on a mixture of multiple task-specific datasets varying in the domain may hamper the matching performance and impede the downstream geometry estimation.

To tackle the above-mentioned challenges, we propose a robust generalist matching network, termed RGM. Specifically, we construct a dense matching framework with a cascaded GRU refinement to fully exploit the geometry similarly with fine-grained features across multiple scales. An extra uncertainty estimation module is also constructed for sparsification. We mix multiple optical flow and sparse matching datasets and carefully design training strategies, including data augmentation, to successfully train our model in a decoupled manner so that the perturbation introduced by diverse domains can be alleviated. We additionally build a dataset with sparse correspondence ground-truth based on the TartanAir ([Wang et al., 2020](#)) dataset to obtain a closer distribution of displacement to those of real-world images.

It is worth mentioning that we design the cascaded GRU refinement module to take advantage of the fine-grained features at a higher resolution. We believe that state-of-the-art methods for optical flow estimation ([Teed & Deng, 2020](#); [Huang et al., 2022](#); [Shi et al., 2023](#); [Xu et al., 2022b](#)) can fit in our framework as well. Our main contributions can be summarized as follows.

- We propose a robust, generalist matching (RGM) network, which works for both sparse and dense matching and can generalize well to unseen scenarios. The large-scale training data, the proposed cascaded GRU refinement for dense correspondence estimation and an uncertainty estimation module for sparsification have all contributed to this superior performance.
- We explore the effectiveness of scaling up the training data by mixing up multiple datasets. A comprehensive analysis is conducted to design a successful training strategy in order to achieve robustness.
- Our RGM achieves state-of-the-art generalization performance in *zero-shot evaluation* for both matching and geometry estimation across multiple datasets, outperforming previous generalist and specialized models by a considerable margin.

## 2 Related Work

Here we review some relevant work that is closest to ours.

### 2.1 Sparse Feature Matching

For a long time, solving the geometry estimation problem has been dominated by sparse correspondence matching methods. Classic methods (Rublee et al., 2011; Liu et al., 2010) propose robust hand-crafted local features for matching and have been adopted in many 3D reconstruction related tasks. Following the manner of detection and matching, learning-based methods efficiently improve the matching accuracy, among which SuperGlue (Sarlin et al., 2020) is a representative network. Given two sets of interest points as well as the corresponding descriptors, SuperGlue utilizes a Transformer-based graph neural network for feature enhancement and to obtain great improvement. LightGlue (Lindemberger et al., 2023) further modifies the SuperGlue by proposing an adaptive strategy due to the matching difficulty which effectively accelerates the inference.

Since the introduction of LoFTR (Sun et al., 2021), detector-free local feature matching methods, which discard the feature detector stage, attract great research attention (Wang et al., 2022; Chen et al., 2022; Tang et al., 2022). LoFTR (Sun et al., 2021) takes a coarse-to-fine strategy by first establishing a dense matching correspondence and removing the unreliable matches at the refinement stage. Self-attention and cross-attention with the transformer are introduced to enlarge the receptive field. Subsequent works propose to improve upon LoFTR. For example, ASpanFormer (Chen et al., 2022) adopts a novel self-adaptive attention mechanism guided by the estimated flow while QuadTree (Tang et al., 2022) primarily focuses on the optimization of attention mechanism by selecting the sparse patches with the highest top  $K$  attention scores for attention computation at the next level such that the computation cost can be efficiently reduced. Sparse correspondence matching plays an important role in geometry estimation including pose estimation, and 3D reconstruction. Unfortunately, the sparsification of matching estimation impedes its applications when all-paired matches are required. Recently, some sparse matching works (Edstedt et al., 2023; Ni et al., 2023; Li et al., 2020; Truong et al., 2021; 2023) are proposed on the base of dense matching where the all-paired matching results are preserved along with a selecting module for sparsification. This is a milestone step towards the generalist matching model.

### 2.2 Dense Matching

For dense correspondence matching, one can categorize them into multiple specific tasks containing stereo matching (Zhang et al., 2021; Chang & Chen, 2018; Xu & Zhang, 2020; Li et al., 2022; Xu et al., 2022a; Lipson et al., 2021), multi-view stereo matching (Ma et al., 2022), and optical flow estimation (Dosovitskiy et al., 2015; Ilg et al., 2017; Sun et al., 2017; Teed & Deng, 2020; Xu et al., 2022b; Huang et al., 2022; Shi et al., 2023; Sui et al., 2022).

Dense correspondence matching is required to provide matching prediction per pixel even in occluded regions which are usually neglected in the sparse matching problem. Among dense matching, optical flow estimation is relatively more challenging due to the disordered motions. The recent work RAFT (Teed & Deng, 2020) proposes a GRU-based iterative mechanism for refining the estimated optical flow by looking up the correlation pyramid repeatedly. RAFT has inspired a few methods for

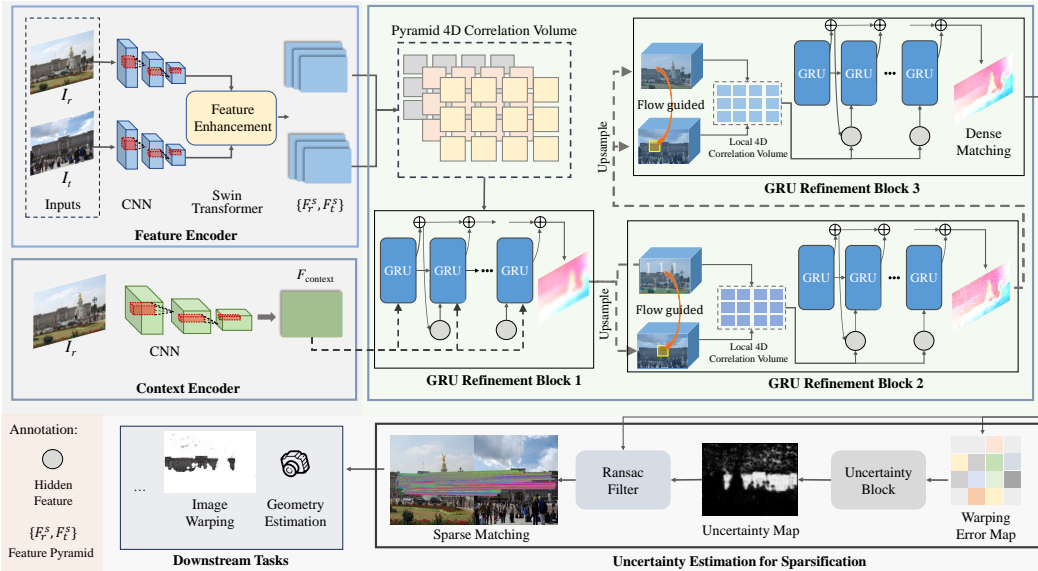


Figure 2: **An overview of our proposed RGM method**, which consists of a pure dense matching network with our cascaded GRU refinement (the upper-right part in shallow green) along with an uncertainty estimation module for sparsification. Some operations such as the skip connection is omitted here for visual clarity.

various dense matching tasks besides the optical flow estimation (Huang et al., 2022; Shi et al., 2023; Jiang et al., 2021; Dong et al., 2023) including MVS (Ma et al., 2022), stereo matching (Li et al., 2022; Lipson et al., 2021), which validates its capacity as a universal architecture for dense matching. The limitation for dense matching lies in that only limited real-world datasets with constrained variation in perspectives are available which may hamper the generalization performance.

### 2.3 Generalist Correspondence Matching

To mitigate the limitation of specialized matching models and unify the matching problems, some attempts have been proposed. MatchFlow (Dong et al., 2023) manages to improve the robustness of optical flow estimation by utilizing a model pretrained on real-world datasets. UniMatch (Xu et al., 2023) proposes to unify the estimation for optical flow, stereo matching, and depth estimation. Note that they tend to fail in the cases of sparse feature matching tasks and/or significant changes of view-point. DKM (Edstedt et al., 2023) and PATS (Ni et al., 2023) are competent for unified matching. They are trained using solely the sparse matching datasets. There is room for improving the performance with dense matching datasets. PDCNet and PDCNet+ (Truong et al., 2021; 2023) propose a universal matching framework with training on both sparse matching datasets and *synthesized* optical flow datasets. Note that, the influence of joint learning of both matching and uncertainty on the mixed datasets of diverse domains remains unexplored.

## 3 Method

We present our method in this section.

### 3.1 Matching Network

As discussed above, the target distribution of displacement magnitude differs in various matching tasks. To unify both dense matching and sparse feature matching, it is crucial to exploit global and local geometry correspondence which requires careful design. We formulate the universal matching as a dense matching problem following an uncertainty estimation module for sparsification. The dense matching  $f$  is defined in the definition of optical flow.

The milestone work of RAFT (Teed & Deng, 2020) provides an appealing approach as the multi-scale correlation pyramid effectively enlarges the receptive field and the iterative looking-up operation associated with contextual information helps with the local correlation exploration. The vanilla RAFT and subsequent variants (Huang et al., 2022; Shi et al., 2023), however, suffer from the utilization of a coarse feature at  $1/8$  resolution which leads to an inevitable loss of fine-grained features. To alleviate this issue, we first construct a feature pyramid network to obtain a set of reference and target features  $\{F_r^s, F_t^s\}$  at the corresponding scales  $s$  of  $\{1/8, 1/4, 1/2\}$  as illustrated in the upper-right block of Fig. 2. We adopt self-attention and cross-attention based on the Swin-Transformer for feature enhancement as in GMFlow (Xu et al., 2022b) at the first two scales.

To adapt to higher resolutions, a cascaded GRU refinement module is proposed. Instead of building all-paired correlations across every scale (Li et al., 2022; Jahedi et al., 2022), the all-paired correlation volume  $C_{full}$  is only introduced at the coarsest resolution of  $1/8$  while the subsequent correlation volume is formulated locally. The all-paired correlation volume  $C_{full}$  is formulated as follows:

$$C_{full} = \frac{F_r F_t^T}{\sqrt{D}} \in \mathbb{R}^{\frac{H}{8} \times \frac{W}{8} \times \frac{H}{8} \times \frac{W}{8}}, \quad (1)$$

where  $(H, W)$  is the spatial resolution of the original image and  $D$  denotes the feature dimension. See GMFlow (Xu et al., 2022b).

A correlation pyramid is then constructed with an additional average pooling operation as RAFT. Given the current flow estimation  $f(x)$  at grid  $x$ , the local correlation with the radius  $r$  is built as:

$$C_{local}(x) = \frac{F_r(x) F_t^T(\mathcal{N}(x + f(x))_r)}{\sqrt{D}}, \quad (2)$$

where  $\mathcal{N}(x)_r$  is the set of local grids centered at  $x$  within radius  $r$  defined as:

$$\mathcal{N}(x)_r = \{x + dx | dx \in \mathbb{Z}^2, \|dx\|_1 \leq r\}. \quad (3)$$

Rather than initializing the hidden status at each scale (Jahedi et al., 2022; Li et al., 2022), we upsample hidden features with bilinear interpolation and pass it to the next refinement stage. Given the correlation as well as the contextual information, we compute motion features as in the vanilla RAFT and feed it to cascaded GRU refinement for flow residual estimation which is then used for updating the matching flow in an iterative manner. We use the  $L_1$  loss for supervision across multiple scales between the matching prediction and ground truth:

$$L_m = \sum_{s=1}^S \gamma_s \begin{cases} \|f_s - f_{gt}\|_1 & \text{if dense matching} \\ \|f_s - f_{gt}\|_1 \odot p & \text{if sparse matching} \end{cases}, \quad (4)$$

where  $p$  indicates the valid mask where sparse correspondence ground truth is available and  $\lambda_s$  is a scalar for adjusting the loss weight at scale  $s$ . We supervise all predicted matches on the optical flow datasets and valid estimated matches on sparse feature matching datasets.

### 3.2 Decoupled Uncertainty Estimation

The indispensable component that unifies the matching problem is the uncertainty estimation module, as discussed in (Truong et al., 2021; Edstedt et al., 2023; Truong et al., 2023; Li et al., 2020). Conventional methods which estimate the valid mask simultaneously with correspondence yield unsatisfactory performance when trained on multiple dataset jointly.

We argue that the joint learning strategy may introduce inevitable noise as the valid mask is closely associated with the matching prediction being inaccurate and ambiguous, especially at the early stage of training. It is an ill-posed problem to determine valid areas given predicted matches of low quality. Moreover, the domain of invalid matches that are filtered out for downstream pose estimation may differ from the occluded regions in optical flow estimation. As we will discuss in Section 4.2, the joint learning of matching and uncertainty could impede the performance of one or both tasks, especially when training on a mixture of datasets.

To alleviate this problem, we decouple our universal matching model into a pure dense correspondence network defined in Subsection 3.1 accompanied by an independent uncertainty estimation

network. As shown in Fig. 2. After obtaining the dense correspondence results, the matching network is frozen. We compute the difference by warping the feature map and the RGB image of the target view to the reference view according to the estimated flow. The uncertainty prediction  $\hat{p}$  is then computed by feeding the warping difference to a shallow convolution network and supervised by valid mask ground truth  $p$  with binary cross-entropy:

$$L_u = \sum_{x,y} p \log(\hat{p}) + (1 - p) \log(1 - \hat{p}). \quad (5)$$

The uncertainty module is only applied at the sparsification stage for the downstream geometry estimation task. We follow the balanced sampling strategy proposed in DKM (Edstedt et al., 2023) to sample valid points within the uncertainty threshold for loss calculation.

### 3.3 Synthesized Optical Flow with Large Intervals

To further exploit the advantages of fine-annotated synthetic datasets but with *significant displacement*, we randomly sample frames with great intervals from 15 to 30 pixels on the TartanAir dataset. Given the provided intrinsic metrics as well as the depth, we first project the reference frame from 2D pixels to 3D point clouds and then reproject to 2D pixels of the target view according to the extrinsic metric.

The matching ground truth  $f_{r \rightarrow t}$  is computed as the difference between the projected and original pixel coordinates. To access the valid mask  $p$  for sparse supervision, the same procedure is repeated from the target view to the reference view and obtain the inverse matching ground truth  $f_{t \rightarrow r}$  such that the forward-backward consistency check (Meister et al., 2018; Xu et al., 2022b) can be applied:

$$p = |f_{r \rightarrow t}(x) + f_{t \rightarrow r}(x + f_{r \rightarrow t}(x))|^2 < \alpha_1 (|f_{r \rightarrow t}(x)|^2 + |f_{t \rightarrow r}(x + f_{r \rightarrow t}(x))|^2) + \alpha_2, \quad (6)$$

where  $\alpha_1$  is 0.05 and  $\alpha_2$  is 0.5. We synthesize around 0.7M training image pairs over 369 scenarios to construct a new dataset named TartanAir Sampled (TS). Note that the synthesized dataset is only used at the stage of matching with sparse ground truth. More details can be found in Appendix A.1.

## 4 Experiment

### 4.1 Implementation Details

Our proposed RGM is trained in a two-stage manner. At the stage of correspondence learning, we first use the MegaDepth (M) (Li & Snavely, 2018) dataset with sparse correspondence ground truth for 200K iterations on a sub-split of 1.4 Million pairs of data. Then we collect additional training data containing the ScanNet (Sc) (Dai et al., 2017), FlyingThings3D (T) (Mayer et al., 2016), and original TartanAir (TA) (Wang et al., 2020) datasets as well as our generated TartanAir Sampled dataset (TS) along with the MegaDepth, reaching a total amount of around 4 Million pairs of images as the training data.

The network is trained for 240K iterations on the mixed dataset. We follow GMFlow (Xu et al., 2022b) with the setting of the AdamW (Loshchilov & Hutter, 2017) optimizer and the cosine learning rate schedule as well as the data augmentation for optical flow related datasets (T, TA, TS). For both the MegaDepth and ScanNet datasets, the input training images are directly resized to  $384 \times 512$  while the rest training data are cropped to the same resolution. The training batch size is set to 16 with a learning rate of  $2e-4$  for the above two rounds of training. We further fine tune the matching network for another 200K iterations at the resolution of  $512 \times 704$  with a batch size of 8 and the initial learning rate is decreased to  $1e-5$ .

At the stage of uncertainty learning, the parameters of the dense matching network are frozen. We train the uncertainty estimation module on the mixture of both MegaDepth and ScanNet datasets for 2 epochs with a batch size of 4 and the learning rate is  $1e-4$ . The related GRU iterations are  $\{7, 4, 2\}$  as we gradually recover the resolution for training and ablation experiments with a corresponding searching radius of  $\{4, 4, 2\}$ . When comparing with other approaches, the iterations increase to  $\{12, 12, 2\}$  which is a closer amount of refinement, compared to RAFT-based methods (Huang et al., 2022; Teed & Deng, 2020; Li et al., 2022; Sui et al., 2022).

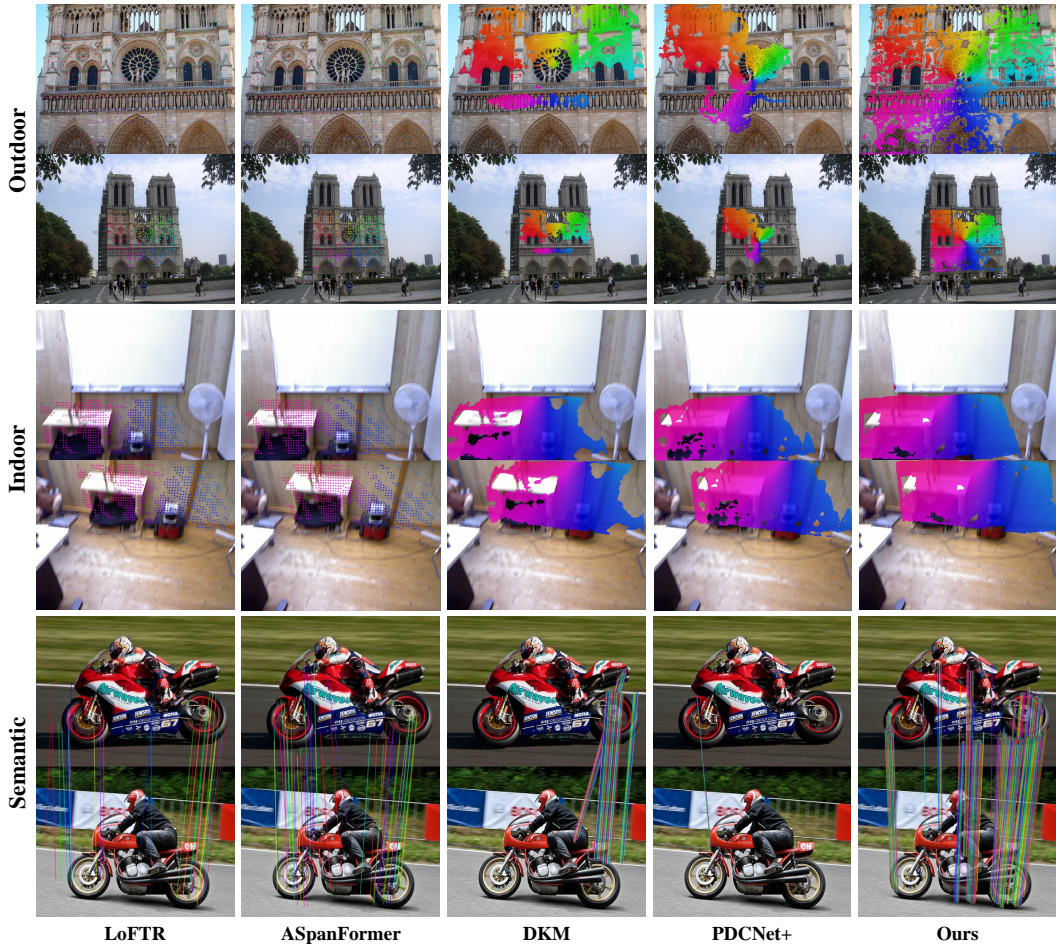


Figure 3: **Visualized comparisons.** Our RGM shows superior performance by obtaining more matches given a pair of indoor or outdoor images. Moreover, our method shows the potential for robust semantic correspondence as well. The same color indicates the matched features.

**Evaluation Metrics:** We report the average end-point-ep (AEPE, lower the better) and percentage of correct key points (PCK-T, higher the better) within a specific pixel threshold  $T$ . F1 metric (lower the better) is reported for the KITTI (Menze & Geiger, 2015) dataset which depicts the percentage of outliers averaged over all valid pixel of the dataset. For pose estimation, we follow previous works (Truong et al., 2021; Sun et al., 2021; Edstedt et al., 2023; Ni et al., 2023) by solving the essential matrix given the corresponding pixels. The accuracy is measured by AUC (higher the better) across different thresholds ( $5^\circ, 10^\circ, 20^\circ$ ).

**Evaluation Datasets:** To validate the generalization performance of our RGM, we perform *zero-shot evaluation* on multiple benchmark datasets containing the ETH3D (Schöps et al., 2017), HPatches (Balntas et al., 2017), KITTI (Menze & Geiger, 2015), and TUM (Sturm et al., 2012) datasets for correspondence estimation. The downstream pose estimation is conducted on the TUM (Sturm et al., 2012) and YFCC (Thomee et al., 2016) datasets. The geometry estimation results are also reported on the ScanNet (Dai et al., 2017) and MegaDepth (Li & Snavely, 2018) datasets. We further adopt the Sintel (Butler et al., 2012) dataset to compare the performance of optical flow estimation under a standard training setting as can be found in Appendix A.3.

## 4.2 Ablation Study

**Network Architecture and Training Strategy:** As presented in Table 1, we analyze the effectiveness of the feature enhancement and the training strategy. The baseline is set as the joint learning of

Table 1: **Ablation experiments on the training components and strategies.** Here ‘w.’ indicates the feature enhancement is utilized and ‘w.o.’ represents removing feature enhancement. It is clear that the independent learning strategy improves generalization performance in matching and pose estimation with the help of feature enhancement.

Method	Dataset	Pose Estimation		Correspondence Matching		
		Megadepth	YFCC	Megadepth	HPatches	ETH3D
		AUC@5°	AUC@5°	PCK-1	AEPE	AEPE
Joint-Learning						
w.o.	M	54.3	48.0	60.8	74.5	2.3
w.	M	55.3	48.2	<b>78.3</b>	31.1	4.2
w.	M + TS	51.9	47.8	77.4	19.2	2.2
Decoupled-Learning						
w.	M	<b>55.7</b>	<b>48.5</b>	78.2	24.9	2.3
w.	M + TS	54.0	48.2	77.3	<b>16.6</b>	<b>2.0</b>

Table 2: **Ablation study on the effectiveness of scaling up training data.** We perform zero-shot matching evaluations as we gradually scale up the training data for diversity increment. Obviously, the employment of numerous training data brings significant generalization improvement.

Dataset	HPatches		KITTI		ETH3D	
	AEPE	PCK-1	AEPE	F1	AEPE	PCK-1
C+T	55.3	38.3	5.4	13.9	3.9	55.0
M	24.9	44.8	12.6	18.4	2.2	50.6
M+Sc	15.3	42.8	10.8	17.7	<b>2.0</b>	54.1
M+Sc+T+TA	<b>13.1</b>	44.3	4.1	10.8	<b>2.0</b>	55.9
M+Sc+T+TA+TS	13.3	<b>46.3</b>	<b>3.5</b>	<b>9.6</b>	<b>2.0</b>	<b>56.3</b>

both matching and uncertainty with feature enhancement on the MegaDepth dataset (Li & Snavely, 2018). Obviously, after removing the self-attention and cross-attention, the network suffers a significant degeneration in matching performance which validates its importance. Directly training on the mixed datasets may improve the matching generalization, but the pose estimation suffers an obvious drop on both the MegaDepth and YFCC (Thomee et al., 2016) datasets although the matching accuracy remains almost unchanged on the MegaDepth, which we attribute to the domain gap between the synthesized images and real-world data for uncertainty estimation.

To validate our hypothesis, we decouple the learning process by learning an independent uncertainty module detached from the learning of similarity. The matching network is trained separately on the MegaDepth and mixed datasets, respectively. The uncertainty estimation is next trained solely on the MegaDepth dataset. The advantage of the decoupled training strategy is easy to see as the matching performance achieves further boost, reaching the lowest AEPE metric (16.6) on the HPatches dataset (Balntas et al., 2017). Compared with the joint learning on the mixed datasets, the decoupled training strategy improves the AUC@5° metric from 51.9 and 47.8 to 54.0 and 48.2 on the Megadepth and YFCC datasets, respectively.

**Scaling Up Training Data.** It is clear from Table 2 that as we scale up the diversity of training data, the generalization performance of correspondence matching improves significantly. Due to the synthesized training data (Dosovitskiy et al., 2015; Mayer et al., 2016) and limited changes of viewpoint, the poor generalization performance from the optical flow estimation is expected.

The accuracy is clearly improved as the training datasets switch to the real-world MegaDepth (Li & Snavely, 2018). We then fine tune the model on the mixture of different datasets for 1 epoch separately. The introduction of the real-world indoor ScanNet (Dai et al., 2017) dataset brings overall improvements on the HPatches (Balntas et al., 2017) and ETH3D (Schöps et al., 2017) datasets indicated by the decreasing average end-point error.

Table 3: **Comparison with other methods for zero-shot matching evaluations.** Specialized models for optical flow estimation and dense-based geometry estimation methods as well as the universal matching models are compared on multiple datasets. Our proposed RSDM achieves the best performance among all the competing approaches. Only the underlined results are obtained with optical flow models trained on the FlyingChairs and FlyingThings3D datasets while others are tested with additional training for Sintel submission. \* indicates we utilize the officially released model and code for evaluations at the original resolution except that we fix the maximum resolution to  $920 \times 1360$  for FlowFormer (Huang et al., 2022) and  $860 \times 1260$  for FlowFormer++ (Shi et al., 2023) due to the computation memory cost.

Method	Task	HPatches		TUM		ETH3D		KITTI
		AEPE	PCK-1	AEPE	PCK-1	AEPE	PCK-1	F1
<i>Specialized models</i>								
RAFT* (Teed & Deng, 2020)	OF	60.8	36.0	8.5	11.6	6.7	48.7	<u>17.4</u>
FlowFormer* (Huang et al., 2022)	OF	81.8	31.7	7.4	11.5	4.9	47.8	<u>14.7</u>
FlowFormer++* (Shi et al., 2023)	OF	81.4	28.5	6.8	11.4	3.5	48.1	<u>14.1</u>
UniMatch* (Xu et al., 2023)	OF	40.5	37.6	6.5	11.6	3.5	50.1	<u>17.6</u>
DKM* (Edstedt et al., 2023)	GE	19.0	34.7	6.1	10.3	2.2	50.1	21.0
<i>Generalist models</i>								
GLUNet* (Truong et al., 2020)	-	25.1	39.6	6.7	10.4	4.4	31.6	37.5
PDCNet+(D)* (Truong et al., 2023)	-	17.5	44.9	4.9	11.5	2.3	53.3	12.6
Ours	-	<b>8.8</b>	<b>47.9</b>	<b>4.1</b>	<b>12.3</b>	<b>2.0</b>	<b>56.4</b>	<b>10.9</b>

When the optical flow datasets are further mixed, the average end-point-error and percentage of outliers accordingly drop from 10.8 to 4.1 and 17.7% to 10.8% on the KITTI dataset (Menze & Geiger, 2015), and the PCK-1 metric goes up to 55.9% on the ETH3D datasets. The performance on the HPatches dataset obtains further boost as the AEPE metric reaches the lowest result. *This improvement of generalization over every testing dataset emphasizes the importance of collecting fine-annotated optical flow datasets to improve the diversity.*

After the employment of our synthesized dataset, the PCK-1 metric reaches 46.3% on the HPatches and the percentage of outliers decreases to 9.6% on the KITTI dataset, surpassing the baseline by 47.8%. Our synthesized TartanAir Sampled dataset also helps to obtain the best matching performance on the ETH3D dataset whose PCK-1 metric rises from 50.6% to 56.3% compared with training solely on the MegaDepth dataset.

### 4.3 Comparisons with Recent Methods

We divide the competing matching methods into two categories: specialized models and generalist models depending primarily on their targeted tasks and the training data. Only sparse ground truth in valid regions is available on the HPatches (Balntas et al., 2017) and ETH3D (Schöps et al., 2017) datasets while the occluded regions are also taken into consideration on the KITTI (Menze & Geiger, 2015) dataset.

**Zero-shot Correspondence Matching.** We conduct experiments to compare the generalization capacity for zero-shot evaluation and present the results in Table 3. The specialized models for optical flow estimation achieve relatively better performance on the KITTI dataset due to the all-paired supervision strategy and the densely annotated datasets but suffer a significant degeneration when switching to real-world scenarios as reflected by the great average end-point error and the poor percentage of correct matches.

The accuracy on the HPatches dataset is promoted when the geometry estimation methods trained on the MegaDepth dataset are adopted whose AEPE drops from 60.8% to 27.1% for DKM compared with RAFT and increases the PCK-1 by 7%. However, the limitation of geometry estimation works lies in their performance on the KITTI dataset due to the incapacity of occluded regions and the relatively coarse annotations. Taking advantage of training data with greater diversity, the generalist models show a balanced performance. Among all the competing methods, *our proposed RGM*

Table 4: **Downstream pose estimation.** We conduct geometry estimation on the YFCC and TUM datasets for zero-shot evaluations. Results on the ScanNet validation set are also reported. Our method achieves the best performance for generalization comparisons.

Method	ScanNet (AUC)			YFCC (AUC)			TUM (AUC)		
	@5°	@10°	@20°	@5°	@10°	@20°	@5°	@10°	@20°
LoFTR (Sun et al., 2021)	22.0	40.8	57.6	42.4	62.5	77.3	-	-	-
DRCNet (Li et al., 2020)	7.7	17.9	30.5	29.5	50.1	66.8	-	-	-
MatchFormer (Wang et al., 2022)	24.3	43.9	61.4	53.3	69.7	81.8	-	-	-
ASpanFormer (Chen et al., 2022)	25.6	46.0	63.3	44.5	63.8	78.4	-	-	-
PATS (Ni et al., 2023)	26.0	46.9	64.3	47.0	65.3	79.2	-	-	-
DKM (Edstedt et al., 2023)	<b>29.4</b>	<b>50.7</b>	<b>68.3</b>	46.5	65.7	80.0	15.5	29.9	46.1
PDCNet+(H) (Truong et al., 2023)	20.3	39.4	57.1	37.5	58.1	74.5	11.0	23.9	40.7
Ours	26.0	46.4	63.9	<b>48.0</b>	<b>66.7</b>	<b>80.5</b>	<b>16.3</b>	<b>31.4</b>	<b>48.4</b>

reaches the best generalization performance over all three datasets. Compared with the second best method PDCNet+ (Truong et al., 2023), our RGM improves the PCK-1 from 44.9% to 47.9% and 53.3% to 56.4% on the HPatches and ETH3D dataset, respectively. Our universal matching work still obtains the best performance on the KITTI dataset.

**Geometry Estimation.** We perform pose estimation on the TUM (Sturm et al., 2012) and YFCC (Thomee et al., 2016) datasets for zero-shot evaluation. The performance on the ScanNet (Dai et al., 2017) dataset is also reported in Table 4. The evaluation of the TUM dataset is only conducted for DKM and PDCNet+ datasets considering the overall generalization performance and access to the official implementation. *Our approach demonstrates the best generalization performance when applying to unseen scenarios*, whether indoor (TUM) or outdoor (YFCC) as assessed by the AUC metric at multiple thresholds.

## 5 Conclusion

In this paper, we have proposed a robust sparse and dense matching network termed RGM incorporating a new cascaded GRU refinement module along with an uncertainty estimation module for sparsification. The decoupled training mechanism as well as the increasing diversity of the numerous training data contributes to our superior generalization performance in zero-shot evaluations for both matching and pose estimation. We will further scale up the training data and optimize the performance of downstream geometry estimation.

## References

- Vassileios Balntas, Karel Lenc, Andrea Vedaldi, and Krystian Mikolajczyk. HPatches: A benchmark and evaluation of handcrafted and learned local descriptors. In *Proc. IEEE Conf. Comp. Vis. Patt. Recogn.*, pp. 5173–5182, 2017.
- Shariq Farooq Bhat, Reiner Birkl, Diana Wofk, Peter Wonka, and Matthias Müller. Zoedepth: Zero-shot transfer by combining relative and metric depth. *arXiv preprint arXiv:2302.12288*, 2023.
- D. J. Butler, J. Wulff, G. B. Stanley, and M. J. Black. A naturalistic open source movie for optical flow evaluation. In A. Fitzgibbon et al. (Eds.) (ed.), *Proc. Eur. Conf. Comp. Vis.*, Part IV, LNCS 7577, pp. 611–625. Springer-Verlag, October 2012.
- Jia-Ren Chang and Yong-Sheng Chen. Pyramid stereo matching network. In *Proc. IEEE Conf. Comp. Vis. Patt. Recogn.*, pp. 5410–5418, 2018. doi: 10.1109/CVPR.2018.00567.
- Hongkai Chen, Zixin Luo, Lei Zhou, Yurun Tian, Mingmin Zhen, Tian Fang, David Mckinnon, Yanghai Tsin, and Long Quan. ASpanFormer: Detector-free image matching with adaptive span transformer. In *Proc. Eur. Conf. Comp. Vis.*, 2022.

- Angela Dai, Angel X Chang, Manolis Savva, Maciej Halber, Thomas Funkhouser, and Matthias Nießner. Scannet: Richly-annotated 3d reconstructions of indoor scenes. In *Proc. IEEE Conf. Comp. Vis. Patt. Recogn.*, pp. 5828–5839, 2017.
- Qiaole Dong, Chenjie Cao, and Yanwei Fu. Rethinking optical flow from geometric matching consistent perspective. In *Proc. IEEE Conf. Comp. Vis. Patt. Recogn.*, pp. 1337–1347, 2023.
- A. Dosovitskiy, P. Fischer, E. Ilg, P. Häusser, C. Hazirbas, V. Golkov, P. v. d. Smagt, D. Cremers, and T. Brox. FlowNet: Learning optical flow with convolutional networks. In *Proc. IEEE Int. Conf. Comp. Vis.*, pp. 2758–2766, 2015.
- Johan Edstedt, Ioannis Athanasiadis, Marten Wadenback, and Michael Felsberg. DKM: Dense kernelized feature matching for geometry estimation. In *Proc. IEEE Conf. Comp. Vis. Patt. Recogn.*, 2023.
- Zhaoyang Huang, Xiaoyu Shi, Chao Zhang, Qiang Wang, Ka Chun Cheung, Hongwei Qin, Jifeng Dai, and Hongsheng Li. FlowFormer: A transformer architecture for optical flow. In *Proc. Eur. Conf. Comp. Vis.*, pp. 668–685, 2022.
- Eddy Ilg, Nikolaus Mayer, Tonmoy Saikia, Margret Keuper, Alexey Dosovitskiy, and Thomas Brox. FlowNet 2.0: Evolution of optical flow estimation with deep networks. In *Proc. IEEE Conf. Comp. Vis. Patt. Recogn.*, pp. 1647–1655, 2017.
- Azin Jahedi, Lukas Mehl, Marc Rivinius, and Andrés Bruhn. Multi-scale raft: Combining hierarchical concepts for learning-based optical flow estimation. In *Proc. IEEE Int. Conf. Image Process.*, pp. 1236–1240, 2022.
- Shihao Jiang, Dylan Campbell, Yao Lu, Hongdong Li, and Richard I. Hartley. Learning to estimate hidden motions with global motion aggregation. In *Proc. IEEE Int. Conf. Comp. Vis.*, pp. 9752–9761, 2021.
- Jiankun Li, Peisen Wang, Pengfei Xiong, Tao Cai, Ziwei Yan, Lei Yang, Jiangyu Liu, Haoqiang Fan, and Shuaicheng Liu. Practical stereo matching via cascaded recurrent network with adaptive correlation. In *Proc. IEEE Conf. Comp. Vis. Patt. Recogn.*, pp. 16263–16272, 2022.
- Xinghui Li, Kai Han, Shuda Li, and Victor Prisacariu. Dual-resolution correspondence networks. *Advances in Neural Information Processing Systems*, 33, 2020.
- Zhengqi Li and Noah Snavely. Megadepth: Learning single-view depth prediction from internet photos. In *Proc. IEEE Conf. Comp. Vis. Patt. Recogn.*, pp. 2041–2050, 2018.
- Philipp Lindenberger, Paul-Edouard Sarlin, and Marc Pollefeys. LightGlue: Local Feature Matching at Light Speed. In *Proc. IEEE Int. Conf. Comp. Vis.*, 2023.
- Lahav Lipson, Zachary Teed, and Jia Deng. RAFT-Stereo: Multilevel recurrent field transforms for stereo matching. In *Int. Conf. 3D Vision (3DV)*, pp. 218–227, 2021.
- Ce Liu, Jenny Yuen, and Antonio Torralba. Sift flow: Dense correspondence across scenes and its applications. *IEEE Trans. Pattern Anal. Mach. Intell.*, 33:978–994, 2010.
- Ilya Loshchilov and Frank Hutter. Decoupled weight decay regularization. In *Proc. Int. Conf. Learn. Representations*, 2017.
- Zeyu Ma, Zachary Teed, and Jia Deng. Multiview stereo with cascaded epipolar raft. In *Proc. Eur. Conf. Comp. Vis.*, 2022.
- Nikolaus Mayer, Eddy Ilg, Philip Häusser, Philipp Fischer, Daniel Cremers, Alexey Dosovitskiy, and Thomas Brox. A large dataset to train convolutional networks for disparity, optical flow, and scene flow estimation. In *Proc. IEEE Conf. Comp. Vis. Patt. Recogn.*, pp. 4040–4048, 2016. doi: 10.1109/CVPR.2016.438.
- Simon Meister, Junhwa Hur, and Stefan Roth. Unflow: Unsupervised learning of optical flow with a bidirectional census loss. In *Proc. AAAI Conf. Artificial Intell.*, volume 32, 2018.

- Iaroslav Melekhov, Aleksei Tiulpin, Torsten Sattler, Marc Pollefeys, Esa Rahtu, and Juho Kannala. Dgc-net: Dense geometric correspondence network. In *Proc. Winter Conf. on Appl. of Comp. Vis.*, pp. 1034–1042. IEEE, 2019.
- M. Menze and A. Geiger. Object scene flow for autonomous vehicles. In *Proc. IEEE Conf. Comp. Vis. Patt. Recogn.*, pp. 3061–3070, 2015.
- Junjie Ni, Yijin Li, Zhaoyang Huang, Hongsheng Li, Hujun Bao, Zhaopeng Cui, and Guofeng Zhang. PATS: Patch area transportation with subdivision for local feature matching. In *Proc. IEEE Conf. Comp. Vis. Patt. Recogn.*, 2023.
- René Ranftl, Katrin Lasinger, David Hafner, Konrad Schindler, and Vladlen Koltun. Towards robust monocular depth estimation: Mixing datasets for zero-shot cross-dataset transfer. *IEEE Trans. Pattern Anal. Mach. Intell.*, 44, 2022.
- Ethan Rublee, Vincent Rabaud, Kurt Konolige, and Gary Bradski. ORB: An efficient alternative to SIFT or SURF. In *Proc. IEEE Int. Conf. Comp. Vis.*, pp. 2564–2571. Ieee, 2011.
- Paul-Edouard Sarlin, Daniel DeTone, Tomasz Malisiewicz, and Andrew Rabinovich. Superglue: Learning feature matching with graph neural networks. In *Proc. IEEE Conf. Comp. Vis. Patt. Recogn.*, pp. 4937–4946, 2020.
- Thomas Schöps, Johannes L. Schönberger, Silvano Galliani, Torsten Sattler, Konrad Schindler, Marc Pollefeys, and Andreas Geiger. A multi-view stereo benchmark with high-resolution images and multi-camera videos. In *Proc. IEEE Conf. Comp. Vis. Patt. Recogn.*, pp. 2538–2547, 2017. doi: 10.1109/CVPR.2017.272.
- Xi Shen, François Darmon, Alexei A Efros, and Mathieu Aubry. Ransac-flow: generic two-stage image alignment. In *Proc. Eur. Conf. Comp. Vis.*, pp. 618–637. Springer, 2020.
- Xiaoyu Shi, Zhaoyang Huang, Dasong Li, Manyuan Zhang, Ka Chun Cheung, Simon See, Hongwei Qin, Jifeng Dai, and Hongsheng Li. Flowformer++: Masked cost volume autoencoding for pre-training optical flow estimation. In *Proc. IEEE Conf. Comp. Vis. Patt. Recogn.*, pp. 1599–1610, 2023.
- J. Sturm, N. Engelhard, F. Endres, W. Burgard, and D. Cremers. A benchmark for the evaluation of RGB-D SLAM systems. In *Proc. IEEE/RSJ Int. Conf. Intelligent Robots and Systems*, 2012.
- Xiuchao Sui, Shaohua Li, Xue Geng, Yan Wu, Xinxing Xu, Yong Liu, Rick Goh, and Hongyuan Zhu. Craft: Cross-attentional flow transformer for robust optical flow. In *Proc. IEEE Conf. Comp. Vis. Patt. Recogn.*, pp. 17602–17611, 2022.
- Deqing Sun, Xiaodong Yang, Ming-Yu Liu, and Jan Kautz. Pwc-net: Cnns for optical flow using pyramid, warping, and cost volume. In *Proc. IEEE Conf. Comp. Vis. Patt. Recogn.*, pp. 8934–8943, 2017.
- Jiaming Sun, Zehong Shen, Yuang Wang, Hujun Bao, and Xiaowei Zhou. LoFTR: Detector-free local feature matching with transformers. In *Proc. IEEE Conf. Comp. Vis. Patt. Recogn.*, pp. 8918–8927, 2021.
- Shitao Tang, Jiahui Zhang, Siyu Zhu, and Ping Tan. Quadtree attention for vision transformers. *Proc. Int. Conf. Learn. Representations*, 2022.
- Zachary Teed and Jia Deng. Raft: Recurrent all-pairs field transforms for optical flow. In *Proc. Eur. Conf. Comp. Vis.*, pp. 402–419, 2020. ISBN 978-3-030-58536-5.
- Bart Thomee, David A Shamma, Gerald Friedland, Benjamin Elizalde, Karl Ni, Douglas Poland, Damian Borth, and Li-Jia Li. Yfcc100m: The new data in multimedia research. *Communications of the ACM*, 59:64–73, 2016.
- Prune Truong, Martin Danelljan, and Radu Timofte. GLU-Net: Global-local universal network for dense flow and correspondences. In *Proc. IEEE Conf. Comp. Vis. Patt. Recogn.*, 2020.

- Prune Truong, Martin Danelljan, Luc Van Gool, and Radu Timofte. Learning accurate dense correspondences and when to trust them. In *Proc. IEEE Conf. Comp. Vis. Patt. Recogn.*, pp. 5710–5720, 2021. doi: 10.1109/CVPR46437.2021.00566.
- Prune Truong, Martin Danelljan, Radu Timofte, and Luc Van Gool. PDC-Net+: Enhanced probabilistic dense correspondence network. *IEEE Trans. Pattern Anal. Mach. Intell.*, 45:10247–10266, 2023.
- Qing Wang, Jiaming Zhang, Kailun Yang, Kunyu Peng, and Rainer Stiefelhagen. MatchFormer: Interleaving attention in transformers for feature matching. In *Proc. Asian Conf. Comp. Vis.*, 2022.
- Wenshan Wang, DeLong Zhu, Xiangwei Wang, Yaoyu Hu, Yuheng Qiu, Chen Wang, Yafei Hu, Ashish Kapoor, and Sebastian Scherer. TartanAir: A dataset to push the limits of visual SLAM. In *Proc. IEEE/RSJ Int. Conf. Intelligent Robots and Systems*, 2020.
- Gangwei Xu, Junda Cheng, Peng Guo, and Xin Yang. Attention concatenation volume for accurate and efficient stereo matching. In *Proc. IEEE Conf. Comp. Vis. Patt. Recogn.*, pp. 12971–12980, 2022a.
- Haofei Xu and Juyong Zhang. AANet: Adaptive aggregation network for efficient stereo matching. In *Proc. IEEE Conf. Comp. Vis. Patt. Recogn.*, pp. 1956–1965, 2020.
- Haofei Xu, Jing Zhang, Jianfei Cai, Hamid Rezaatofghi, and Dacheng Tao. GMFlow: Learning optical flow via global matching. In *Proc. IEEE Conf. Comp. Vis. Patt. Recogn.*, pp. 8121–8130, June 2022b.
- Haofei Xu, Jing Zhang, Jianfei Cai, Hamid Rezaatofghi, Fisher Yu, Dacheng Tao, and Andreas Geiger. Unifying flow, stereo and depth estimation. *IEEE Trans. Pattern Anal. Mach. Intell.*, 2023.
- Wei Yin, Xinlong Wang, Chunhua Shen, Yifan Liu, Zhi Tian, Songcen Xu, Changming Sun, and Dou Renyin. Diversedepth: Affine-invariant depth prediction using diverse data. *arXiv preprint arXiv:2002.00569*, 2020.
- Wei Yin, Chi Zhang, Hao Chen, Zhipeng Cai, Gang Yu, Kaixuan Wang, Xiaozhi Chen, and Chunhua Shen. Metric3D: Towards zero-shot metric 3d prediction from a single image. In *Proc. IEEE Int. Conf. Comp. Vis.*, 2023.
- Songyan Zhang, Zhicheng Wang, Qiang Wang, Jinshuo Zhang, Gang Wei, and Xiaowen Chu. Ednet: Efficient disparity estimation with cost volume combination and attention-based spatial residual. In *Proc. IEEE Conf. Comp. Vis. Patt. Recogn.*, pp. 5429–5438, 2021.

## A Appendix

### A.1 Synthesized TartanAir Sampled Dataset

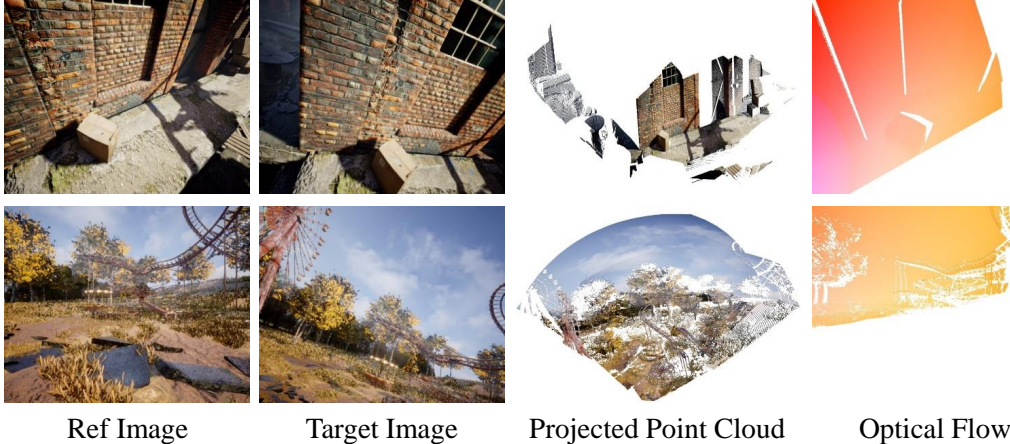


Figure 4: **An overview of our generated optical flow sampled from the TartanAir dataset with large intervals** to imitate the large viewpoint changes in the real world. The associated changes in brightness as well as the scale of objects can be well preserved.

We build a set of training data pairs with sparse correspondence annotations based on the TartanAir dataset. The selected reference and target image samples are visualized in Fig. A.1. The sampling interval is intended to be large for the purpose of significant changes in perspective. We can obtain scale-consistent depth map  $\mathbf{D}_{ref}$ , intrinsic camera parameter  $\mathbf{K}$ , camera-to-world camera pose  $\mathbf{P}_{ref}$  of the reference image and camera-to-world camera pose  $\mathbf{P}_{tar}$  of the target image from original TartanAir dataset. Subsequently, we engage in the projection of pixel coordinates  $(u, v)$  from the reference image into 3D point clouds. These points are then further projected onto their corresponding pixels, contingent upon the camera-to-world camera pose  $\mathbf{P}_{tar}$  of the target image. The process is depicted as follows.

$$(u', v', 1)^T = \mathbf{K}\mathbf{P}_{tar}^T\mathbf{P}_{ref}\mathbf{K}^{-1}\mathbf{D}_{ref}(u, v, 1)^T \quad (7)$$

where  $(u', v')$  is the coordinates of the reference image projected onto the target perspective. After a fundamental coordinate transformation, we can obtain the corresponding grid pairs so that the optical flow in valid regions can be calculated. We subtract the original coordinates  $(u, v)$  from the projected coordinates  $(u', v')$  to obtain the optical flow  $\mathbf{F}$ :

$$\mathbf{F} = (u' - u, v' - v). \quad (8)$$

Compared with the synthesized optical flow utilized in previous works (Truong et al., 2020; 2021), our synthesized data with large displacement can preserve the change of brightness and scale introduced by different perspectives.

### A.2 Dataset Analysis

As shown in Table 5, we count the distribution of the Euclidean distance of correspondence on our training and evaluation datasets. The distribution is divided into three intervals [s0-10, s10-40, s40+] indicating the displacement’s magnitude falling to 0 – 10, 10 – 40 pixels, and more than 40 pixels. The real-world datasets such as HPatches (Balntas et al., 2017), MegaDepth (Li & Snavely, 2018), and ScanNet (Dai et al., 2017) normally contain a dominant ratio of displacement over 40 pixels compared with the synthesized datasets (Butler et al., 2012; Mayer et al., 2016). It is clear that our synthesized dataset obtains a closer distribution to the real-world datasets which contributes importantly to the robustness of our work.

Table 5: **The distribution of correspondence magnitude.** We count the Euclidean distance on real-world (R) datasets including KITTI, HPatches, Megadepth-1500, and synthesized (S) datasets including FlyingThings3D, TartanAir, and our synthesized dataset. Our generated dataset obtains a greater ratio of large displacement. ‘R’ is short for real-world while ‘S’ is short for synthesized.

Datasets	Type	Distance Distribution		
		s0-10	s10-40	s40+
K (Menze & Geiger, 2015)	R	30.3	36.5	33.2
HP (Balntas et al., 2017)	R	0.9	4.5	94.6
T (Mayer et al., 2016)	S	25.2	45.7	29.1
TA (Wang et al., 2020)	S	46.2	47.2	6.6
Si (Butler et al., 2012)	S	69.0	21.3	9.7
Sc (Dai et al., 2017)	R	0.0	0.6	99.4
M (Li & Snavely, 2018)	R	1.1	10.9	88.0
TS (Ours)	S	0.9	9.2	89.9

### A.3 Optical Flow Estimation

We conduct experiments for optical flow estimation to explore the performance of dense-based geometry estimation networks and compare our proposed methods with other state-of-the-art optical flow methods under the same training pipeline.

As reported in Table 6, generalization results on the Sintel and KITTI datasets are reported with training on the FlyingChairs first following the finetune on the FlyingThings3D datasets. It is clear that DKM struggles in disordered motion estimation and obtains close performance to PWCNet (Sun et al., 2017) as they share a close design of network architecture. The proposed iterative GRU refinement in RAFT (Teed & Deng, 2020) empowers the localization of fast-moving objects which is required in optical flow estimation. Our method achieves competitive results on the Sintel dataset and reaches the lowest outlier percentage on the KITTI dataset. As can be seen in Fig. 5, the detailed optical flow prediction can be obtained with the help of the employment of fine-grained features.

Table 6: **Generalization comparison for optical flow estimation.** Following a standard pipeline, we train our RSDM and DKM on FlyingChairs and FlyingThings datasets while testing on Sintel and KITTI datasets. Our RSDM achieves the lowest percentage of matching outliers.

Method	Sintel-EPE		KITTI	
	Clean	Final	EPE	F1
PWCNet (Sun et al., 2017)	2.6	3.9	10.4	33.7
DKM (Edstedt et al., 2023)	2.6	4.4	13.1	37.7
MS-RAFT (Jahedi et al., 2022)	1.4	2.7	-	-
FlowFormer (Huang et al., 2022)	<b>1.0</b>	<b>2.4</b>	<b>4.1</b>	14.7
GMFlow (Xu et al., 2022b)	1.1	2.5	7.8	23.4
RAFT (Teed & Deng, 2020)	1.4	2.7	5.0	17.4
Ours	<b>1.0</b>	<b>2.4</b>	4.6	<b>13.2</b>

### A.4 ETH3D Evaluation

We provide detailed results on ETH3D in Table 7.

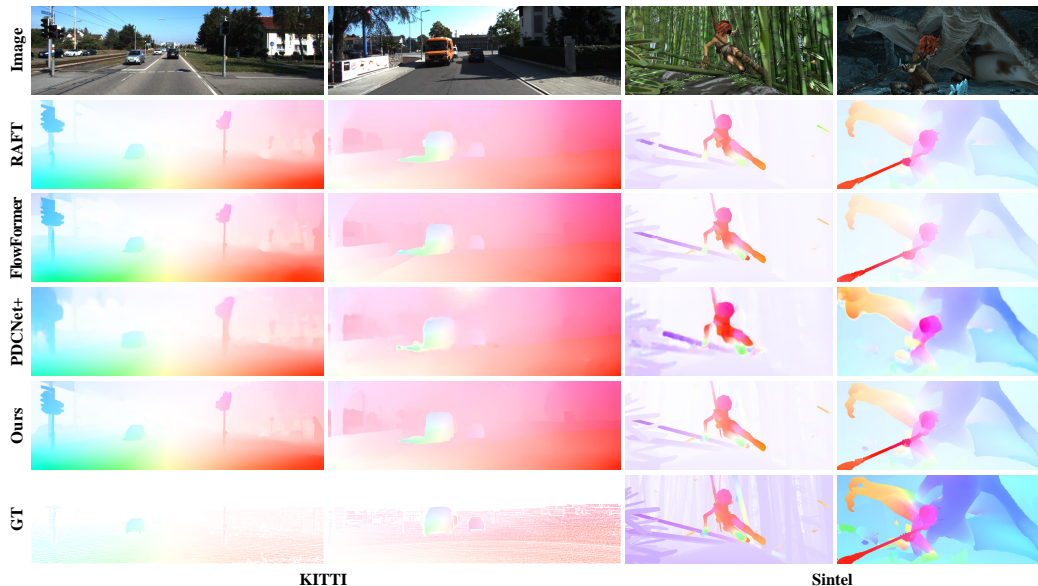


Figure 5: **Qualitative comparison on the KITTI and Sintel datasets.** Our RSDM is capable of estimating more consistent and detailed optical flow compared with others.

Table 7: **Zero-shot evaluation on the ETH3D dataset.** Both average end-point-error and percentage of correct matches within the 1-pixel threshold are reported at various intervals.

Method	5	7	9	11	13	15
	AEPE					
RANSAC-Flow (Shen et al., 2020)	1.9	2.1	2.3	2.4	2.6	2.8
PDCNet+(H) (Truong et al., 2023)	<b>1.7</b>	2.0	2.2	2.5	2.7	3.2
FlowFormer (Huang et al., 2022)	2.0	2.3	2.8	3.3	8.0	13.9
FlowFormer++ (Shi et al., 2023)	2.0	2.2	2.6	3.1	4.0	8.7
RAFT (Teed & Deng, 2020)	1.8	2.1	2.8	5.8	11.7	21.2
DKM (Edstedt et al., 2023)	1.8	1.9	2.1	2.2	2.4	2.6
Ours	<b>1.7</b>	<b>1.8</b>	<b>2.0</b>	<b>2.1</b>	<b>2.3</b>	<b>2.4</b>
PCK-1						
RANSAC-Flow (Shen et al., 2020)	54.7	51.6	48.6	46.1	44.0	41.8
PDCNet+(H) (Truong et al., 2023)	59.9	56.8	54.1	51.6	49.6	47.3
FlowFormer (Huang et al., 2022)	55.1	50.9	47.3	44.0	40.6	37.2
FlowFormer++ (Shi et al., 2023)	55.2	51.1	47.5	44.1	41.2	37.7
RAFT (Teed & Deng, 2020)	56.2	52.0	48.4	44.8	41.3	37.6
DKM (Edstedt et al., 2023)	58.9	56.0	53.4	51.1	49.2	47.1
Ours	<b>60.8</b>	<b>58.2</b>	<b>55.9</b>	<b>53.8</b>	<b>52.0</b>	<b>50.3</b>

## A.5 Visualization

We provide more visualizations here.



Figure 6: More visualized comparisons between our RGM and other methods.